Excitation of Chaotic Spin Waves in Magnetic Film Feedback Rings through Three-Wave Nonlinear Interactions

Aaron M. Hagerstrom,[1] Wei Tong,[1] Mingzhong Wu,[1,*] Boris A. Kalinikos,[2] and Richard Eykholt[1]

[1]*Department of Physics, Colorado State University, Fort Collins, Colorado 80523, USA*

[2]*St. Petersburg Electrotechnical University, 197376, St. Petersburg, Russia*

(Received 31 December 2008; published 18 May 2009)

This Letter reports experimental results on the three-wave interactions of backward volume spin waves in a magnetic film and the excitation of chaotic waves through such interactions in a magnetic film-based active feedback ring. The three-wave interactions manifest themselves in the power saturation responses of spin waves, and the chaotic excitation manifests itself in chaotic waveforms and broad spectra. The fractal dimensions of the chaotic signals are finite and can be controlled by changing the ring gain.

DOI: 10.1103/PhysRevLett.102.207202 PACS numbers: 75.30.Ds, 05.45.−a, 76.50.+g, 85.70.Ge

Three-wave nonlinear interactions can serve as a route to chaotic excitation [1–8]. The experimental demonstration of such an excitation has been carried out in (1) ultrasonic waves in crystals and (2) spin waves in magnetic films. In both cases, the three-wave interactions involved two different types of waves. For (1), the development of the chaos was through the interactions of longitudinal and transverse ultrasonic waves [5]. For (2), the chaos was excited through the interactions between surface and volume spin waves [6–8].

When a magnetic film strip is magnetized to saturation along its length, it supports the propagation of backward volume spin waves [9,10]. These waves are termed ''backward'' because they have negative group velocity in the low wave number region. They can travel ''forward'' when the wave numbers are high. In principle, such spin waves can also undergo three-wave interactions if the magnetic field is set low so that the frequency of a spin wave and its half are both within the frequency band of the allowed wave spectrum. However, such interactions will involve only one and the same type of wave, rather than two types of waves as in previous work [5–8]. In practice, such interactions and the chaotic excitation through them have never been demonstrated.

This Letter reports for the first time (1) the experimental evidence for three-wave interactions of backward volume spin waves and (2) the excitation of chaotic spin waves through these interactions. For (1), one measures the power saturation of backward volume spin waves at low fields. Such saturation responses indicate the occurrence of three-wave interactions. For (2), one measures and characterizes chaotic spin waves that are self-generated in a magnetic film feedback ring. The three-wave interactions involve two parametric processes, a splitting process $\omega_0 = \omega_1 + \omega_2$, where an initial wave of frequency ω_0 produces two new waves with frequencies ω_1 and ω_2 at about $\omega_0/2$, and a confluence process $\omega_1 + \omega_2 = \omega_3$, where two of the parametrically excited waves interact to produce one high-frequency wave ω_3. When the waves are strong, such processes can lead to the generation of many new waves with frequencies close to but different from the initial frequency ω_0, and this leads to the broadening of frequency spectra and the excitation of chaotic waveforms.

It is worth mentioning that there is a lot of previous work on the nonlinear effects of backward volume spin waves, including work on solitons [11], recurrence [12], Bose-Einstein condensation [13], and chaos [14]. For all of these, however, the magnetic fields were set high so that three-wave interactions were prohibited and four-wave interactions were the only underlying nonlinear process. In addition to the work on spin-wave chaos mentioned above [6–8], there are other studies on the three-wave interactions of spin waves [15–19]. In all of them, the three-wave interactions were between surface and volume waves. Note that, in Refs. [8,15,16,18], the three-wave interactions were demonstrated through the power saturation of surface spin waves, while, in Ref. [19], the interactions were demonstrated by measurements of half-frequency volume modes with a Brillouin light scattering (BLS).

The present experiments used a magnetic yttrium iron garnet (YIG) film strip, which was magnetized to saturation by a magnetic field parallel to the strip's length. This field configuration corresponds to the propagation of backward volume spin waves [9,10]. Two microstrip line transducers were placed over the YIG strip to excite and detect spin waves [11]. For the measurements on the spin-wave power saturation, one applied continuous microwaves to the excitation transducer and measured the signals from the detection transducer. For the measurements on chaotic waves, one used a feedback ring configuration where the output signal from the detection transducer was fed back to the excitation transducer through a microwave amplifier and an adjustable microwave attenuator. No external signal was introduced to the ring. The ring signal was sampled through a directional coupler, with feeds to an oscilloscope for temporal measurements and a spectrum analyzer for frequency analysis. Details on the feedback ring can be found in Ref. [20].

For the data presented below, the YIG strip was 5.0 μm thick, 1.88 mm wide, and 60 mm long. It was cut from a

larger YIG film grown on a gadolinium gallium garnet substrate. The microstrip line transducers were 50 μm wide and 2 mm long. Their separation was 5 mm. The amplifier had a 30 dB dynamic range, a peak output power of 2 W, and a linear response from 2 to 8 GHz. This amplifier configuration insures that the nonlinear response of the ring is determined solely by the YIG film.

Figure 1 shows data for the YIG-transducer structure. The left and right columns are for a high field and a low field, respectively. These fields were chosen to illustrate the ''off'' and ''on'' regimes of the three-wave processes. The top panel shows the calculated dispersion curves [21,22]. The solid lines mark the frequency bands of the spin waves excited in the experiments. The corresponding half-frequency bands are marked by dashed lines. In principle, it is possible to excite a large number of spin-wave modes that propagate along the YIG strip but also have nonzero wave vectors normal to the YIG film. In practice, however, only the main mode, the one with the simplest dynamical magnetization distribution across the film thickness, is efficiently excited and measurable, and all of the other modes are very weak in comparison with the main mode [9,23]. The dispersion curves in the top panel are for the main modes. The middle panel shows the transmission responses of the YIG-transducer structure. The black curves and gray empty circles are for the data measured at different input microwave power levels (P_{in}), as indicated. The bottom panel shows the output power (P_{out}) vs input power responses for the same structure. They were measured at different frequencies, as indicated.

Graph (a-i) shows that, at $H = 753$ Oe, the half-frequency cuts of the excited waves are well below the theoretical wave band. However, as the field is reduced to 300 Oe, the dispersion curve shifts downward and the half frequencies are now within the wave band, as in (b-i). These results indicate that the 753 Oe configuration corresponds to a high-field regime where three-wave processes are prohibited, while the 300 Oe configuration corresponds to a low-field regime where three-wave processes are allowed. The data in the middle panel show a perfect match between the two curves for $H = 753$ Oe and a significant difference between the two curves for $H = 300$ Oe. These results indicate that, in the high-field regime, the transmission loss of the waves is power-independent, while, in the low-field regime, the transmission loss strongly depends on the input power. The data also show that the bandwidths of the excited waves (about 50 MHz) are much narrower than the theoretical bandwidths (over 1 GHz). This is associated with the width effect of the transducers and the group velocity properties of the waves [9,10]. The data in (a-iii) and (b-iii) show significantly different responses. For $H = 753$ Oe, the three P_{out}-P_{in} responses are all linear. For $H = 300$ Oe, however, one sees saturation responses.

The data in Fig. 1 provide the first demonstration of three-wave interactions of backward volume spin waves. In the high-field regime, three-wave interactions are not allowed, and the energy of the excited waves cannot dissipate through three-wave processes. As a result, the energy of the spin waves increases linearly with the input power. This accounts for the lack of dependence of the transmission loss on P_{in} shown in (a-ii) and the linear P_{out}-P_{in} responses shown in (a-iii). In the low-field regime, the energy of the spin waves increases linearly with the input power if the power of the spin waves is lower than the threshold for the onset of three-wave processes. If the power is beyond the threshold, the energy of the spin waves will be transferred to the half-frequency modes through a splitting process. As a result, one observes high loss at high power, as shown in (b-ii), and saturation in the P_{out}-P_{in} responses, as shown in (b-iii). Note that the half-frequency modes have very large wave numbers, as shown in (b-i), and, therefore, cannot be probed by the detection transducer [10]. The data in (b-iii) also indicate a power threshold of about -30 dBm. This threshold is much lower than that for the three-wave interactions between backward volume spin waves and surface spin waves [8].

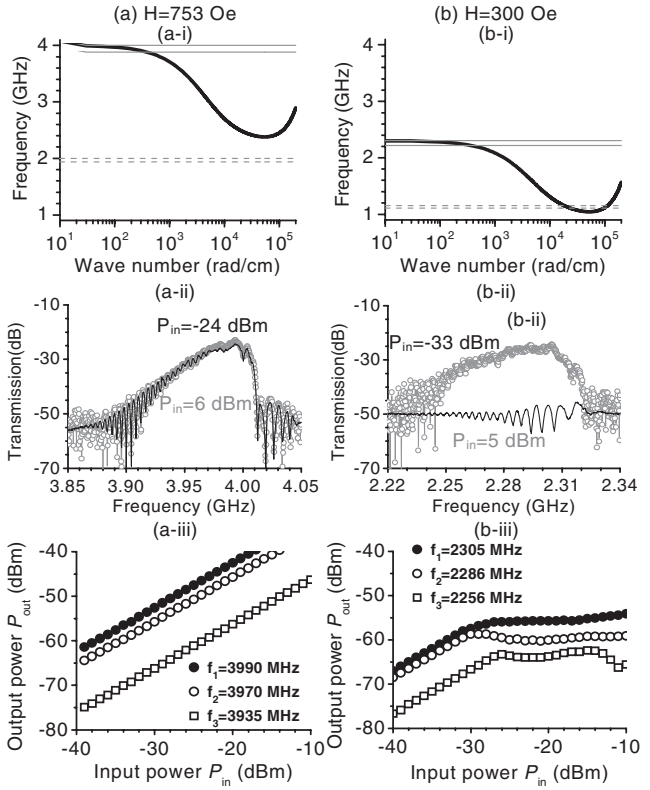

FIG. 1. Evidence for three-wave interactions of backward volume spin waves. The top panel shows the calculated frequency vs wave number dispersion curves. The middle panel shows the measured transmission loss vs frequency curves for a YIG-transducer structure. The bottom panel shows the output power vs input power responses for the same structure. The left and right columns are for different magnetic fields, as indicated.

Turn now to the chaotic excitation through the above-described processes in a ring system. A feedback ring has a number of eigenmodes. Their frequencies are determined

by $k(\omega) \cdot l + \phi_0 = 2\pi n$, where k is the spin-wave wave number, ω is the spin-wave frequency, l is the transducer separation, ϕ_0 is the phase shift introduced by the feedback circuit, and n is an integer. Detailed discussion on these eigenmodes can be found in Refs. [24,25]. At a low ring gain G, all of the eigenmodes experience an overall net loss, and there is no spontaneous signal in the ring. If the ring gain is increased to a certain level, here taken as $G = 0$, the eigenmode with the lowest decay rate will start to self-generate, and one will obtain a continuous wave at this eigenmode frequency. A further increase in G leads to the excitation of additional eigenmodes, enhancement of modes, and subsequent excitation of half-frequency modes through the splitting process. Strong half-frequency modes can also interact to produce new modes through a confluence process. The splitting and confluence processes obey energy conservation, $\omega_0 = \omega_1 + \omega_2$ and $\omega_1 + \omega_2 = \omega_3$, respectively, as well as momentum conservation $\mathbf{k}_0 = \mathbf{k}_1 + \mathbf{k}_2$ and $\mathbf{k}_1 + \mathbf{k}_2 = \mathbf{k}_3$, respectively, where $\mathbf{k}_i$ is the wave vector for the mode of frequency ω_i. The interplay of these processes leads to the production of new modes, the broadening of the spectra, and the excitation of chaotic spin waves.

Figure 2 shows representative ring signals that demonstrate the effects discussed above. The signals were obtained at 300 Oe and different ring gain levels, as indicated. In each panel, the left and right graphs show the power-frequency spectrum and the time-domain waveform, respectively. The insets in (a) and (c) show the corresponding data in expanded horizontal scales.

For $G = 0$, one observes a single frequency peak at 2.295 GHz and a continuous wave in the time domain, as in (a). This corresponds to the self-generation of the eigenmode with the lowest decay rate. As the gain is increased to 1 dB, a new mode appears at 2.287 GHz. This mode and the initial mode interfere to produce a periodic modulation in the waveform, as in (b). One also observes several other eigenmodes in the spectrum, but they are too weak to produce any noticeable responses in the time domain. As the gain is further increased to 1.5 dB, one observes the enhancement and broadening of the peaks in the frequency domain and a chaotic behavior in the time domain, as in (c). Now, each frequency peak does not represent a single frequency but consists of a broad spectrum, as represented in the inset in (c). Additional increases in G lead to the further enrichment of the chaotic dynamics. This is represented in (d).

These results clearly demonstrate the development of chaotic spin waves through the splitting and confluence processes. It is important to emphasize that both the high-frequency and half-frequency waves involved are volume waves. This aspect is different from that in previous work [6–8]. Also, the chaotic spectra are much narrower than those reported in Ref. [8]. This is because the passband for backward volume waves at low fields is narrower than that for surface waves. It is also important to emphasize that four-wave processes do not play a dominant role here.

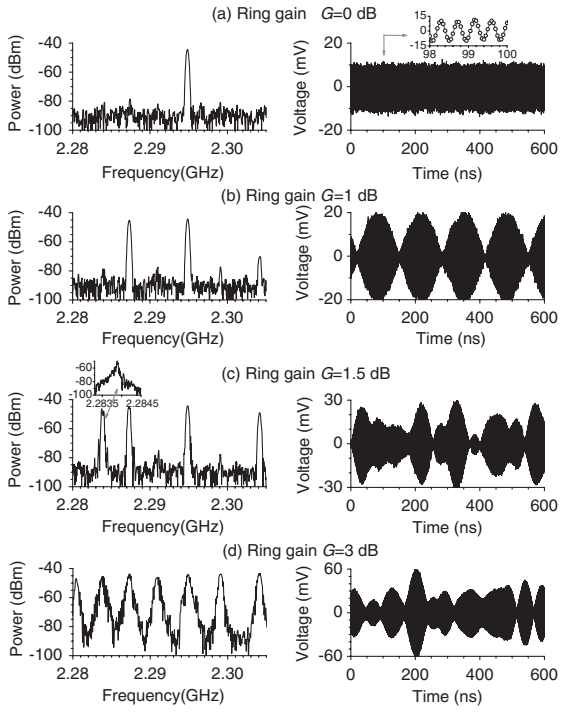

FIG. 2. Ring signals obtained at different ring gain levels as indicated. The left and right graphs show the power vs frequency spectra and the time-domain waveforms, respectively. The insets show the corresponding data in expanded horizontal scales.

There are two reasons. First, four-wave processes usually occur at a power threshold level much higher than that for three-wave processes [26,27]. Second, the main peaks in the frequency spectrum in (d) are unequally spaced, and this indicates that the four-wave processes are not present. With four-wave processes, the frequencies of the new modes should be equally spaced, and the frequency spectra at high ring gain levels should have a uniform comb structure [20,25]. In fact, the central frequencies of all the peaks in (d) match the theoretical ring eigenfrequencies.

Correlation dimensions were computed for the measured chaotic signals [28,29]. This involves the calculation of the fraction of the pairs of points on the attractor whose sup-norm separation is no greater than a probing distance r [30]. This fraction is called the correlation sum C, and a plot of C as a function of r is called a correlation plot. The attractors were constructed through the method of time delays [28,29]. The time delays were determined by the use of a correlation integral approach [30]. The correlation sum C scales with the probing distance r according to $C(r) \propto r^D$, where D is the correlation dimension. One can obtain D by taking the slope of the linear scaling region of the $\log(C)$ vs $\log(r)$ plot.

When one increases the embedding dimension of an attractor, the correlation dimension initially increases and then reaches a limit when the embedding space is large enough for the attractor to untangle itself. This limiting correlation dimension is the fractal dimension of the chaotic signal. The correlation dimension can be used to

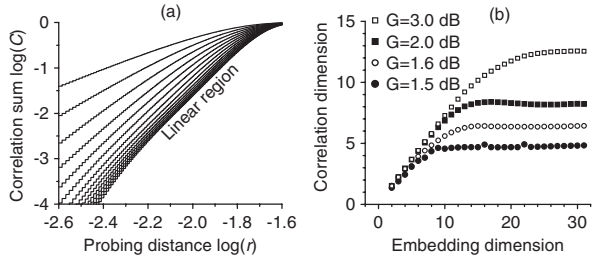

FIG. 3. (a) Correlation plots for the ring signal obtained at $G = 1.5$ dB. From left to right, the embedding dimensions of the plots increase from 2 to 15. (b) Correlation dimension vs embedding dimension responses for the signals obtained at different ring gain levels, as indicated.

distinguish chaotic waves from noise, because noise does not have a finite fractal dimension. As noise fills up the space densely, the corresponding correlation dimension continues to increase with the embedding dimension.

Figure 3 gives representative data. (a) shows the correlation plots for the $G = 1.5$ dB signal. (b) shows the correlation dimension vs embedding dimension responses for the signals obtained at different ring gain levels, as indicated. Note that, for all the calculations, the attractors were constructed from the envelopes of waveforms.

The plots in (a) show a clear linear region as indicated. It was this region where the slopes of the plots were taken to give the correlation dimensions for the $G = 1.5$ dB signal. The responses in (b) all show clear saturation. From these saturation responses, the fractal dimensions of the signals were estimated to be 4.8, 6.3, 8.3, and 12.5 for $G = 1.5$ dB, 1.6 dB, 2 dB, and 3 dB, respectively. These data clearly demonstrate the chaotic nature of the measured signals and the controllability of the dimension of the chaotic signal.

These results reveal a new physical mechanism for the excitation of chaotic microwaves, which is critically needed by chaotic communications [31]. The saturation effect of the spin-wave power can be used to develop power limiters and signal-to-noise enhancers [10,15,16,18]. Also, it is worth noting that the details of the three-wave processes of backward volume spin waves have now been mapped through a BLS technique [32].

This work was supported in part by the U. S. Army Research Office (W911NF-08-1-0476), the U. S. National Science Foundation (ECCS-0725386), and the Russian Foundation for Basic Research (08-02-00959).

*Corresponding author.
mwu@lamar.colostate.edu

[1] S. R. Lopes and A. C.-L. Chian, Phys. Rev. E **54**, 170 (1996).
[2] M. M. Skoric, M. S. Jovanovic, and M. R. Rajkovic, Europhys. Lett. **34**, 19 (1996).
[3] A. C.-L. Chian, F. A. Borotto, S. R. Lopes, and J. R. Abalde, Planet. Space Sci. **48**, 9 (2000).
[4] A. C.-L. Chian, E. L. Rempel, and F. A. Borotto, Nonlinear Proc. Geophys. **9**, 435 (2002).
[5] L. Ilchenko, V. Grimalsky, S. Koshevaya, and G. Burlak, Phys. Lett. A **303**, 169 (2002).
[6] V. E. Demidov and N. G. Kovshikov, Tech. Phys. Lett. **24**, 274 (1998).
[7] V. E. Demidov and N. G. Kovshikov, Tech. Phys. Lett. **24**, 647 (1998).
[8] M. Wu, B. A. Kalinikos, and C. E. Patton, Phys. Rev. Lett. **95**, 237202 (2005).
[9] D. D. Stancil, *Theory of Magnetostatic Waves* (Springer-Verlag, New York, 1993).
[10] P. Kabos and V. S. Stalmachov, *Magnetostatic Waves and Their Applications* (Chapman & Hall, London, 1994).
[11] M. Chen, M. A. Tsankov, J. M. Nash, and C. E. Patton, Phys. Rev. B **49**, 12 773 (1994).
[12] M. M. Scott, B. A. Kalinikos, and C. E. Patton, J. Appl. Phys. **94**, 5877 (2003).
[13] S. O. Demokritov, V. E. Demidov, O. Dzyapko, G. A. Melkov, A. A. Serga, B. Hillebrands, and A. N. Slavin, Nature (London) **443**, 430 (2006).
[14] A. V. Kondrashov, A. B. Ustinov, B. A. Kalinikos, and H. Benner, Tech. Phys. Lett. **34**, 492 (2008).
[15] J. D. Adam and S. N. Stitzer, Appl. Phys. Lett. **36**, 485 (1980).
[16] J. D. Adam and S. N. Stitzer, IEEE Trans. Microwave Theory Tech. **41**, 2227 (1993).
[17] V. T. Synogach, Y. K. Fetisov, C. Mathieu, and C. E. Patton, Phys. Rev. Lett. **85**, 2184 (2000).
[18] J. D. Adam and S. N. Stitzer, IEEE Trans. Magn. **40**, 2844 (2004).
[19] C. Mathieu, V. T. Synogatch, and C. E. Patton, Phys. Rev. B **67**, 104402 (2003).
[20] M. Wu and C. E. Patton, Phys. Rev. Lett. **98**, 047202 (2007).
[21] B. A. Kalinikos, Sov. Phys. J. **24**, 718 (1981).
[22] B. A. Kalinikos and A. N. Slavin, J. Phys. C **19**, 7013 (1986).
[23] V. F. Dmitriev and B. A. Kalinikos, Russ. Phys. J. **31**, 875 (1988).
[24] B. A. Kalinikos, N. G. Kovshikov, and C. E. Patton, Appl. Phys. Lett. **75**, 265 (1999).
[25] M. Wu, B. A. Kalinikos, L. D. Carr, and C. E. Patton, Phys. Rev. Lett. **96**, 187202 (2006).
[26] B. Lax and K. J. Button, *Microwave Ferrites and Ferrimagnetics* (McGraw-Hill, New York, 1962).
[27] A. N. Slavin, J. Phys. IV (France) **7**, C1-379 (1997).
[28] P. S. Addison, *Fractals and Chaos* (Institute of Physics, Bristol, 1997).
[29] H. Kantz and Th. Schreiber, *Nonlinear Time Series Analysis* (University Press, Cambridge, 2004).
[30] H. S. Kim, R. Eykholt, and J. D. Salas, Physica (Amsterdam) **127D**, 48 (1999).
[31] A. S. Dmitriev, B. Y. Kyarginsky, A. I. Panas, and S. O. Starkov, Int. J. Bifurcation Chaos Appl. Sci. Eng. **13**, 1495 (2003).
[32] C. L. Ordóñez-Romero, B. A. Kalinikos, P. Krivosik, W. Tong, P. Kabos, and C. E. Patton, Phys. Rev. B **79**, 144428 (2009).